A CFD-based framework for the analysis of soil-pipeline interaction in re-consolidating liquefied sand

Federico Pisanò, Ph.D. (corresponding author)[1], Massimiliano Cremonesi, Ph.D.[2], Francesco Cecinato, Ph.D.[3], and Gabriele Della Vecchia, Ph.D.[4]

[1]Assistant Professor – Faculty of Civil Engineering and Geosciences, Delft University of Technology, Stevinweg 1, 2628 CN, Delft (The Netherlands).
Email: f.pisano@tudelft.nl

[2]Associate Professor – Department of Civil and Environmental Engineering, Politecnico di Milano, piazza L. da Vinci 32, 20133, Milano (Italy)

[3]Associate Professor – Dipartimento di Scienze della Terra 'A. Desio', Università degli Studi di Milano, via L. Mangiagalli 34, 20133, Milano (Italy)

[4]Associate Professor – Department of Civil and Environmental Engineering, Politecnico di Milano, piazza L. da Vinci 32, 20133, Milano (Italy)

Abstract

Submarine buried pipelines interact with shallow soil layers that are often loose and prone to fluidization/liquefaction. Such occurrence is possible consequence of pore pressure build-up induced by hydrodynamic loading, earthquakes and/or structural vibrations. When liquefaction is triggered in sand, the soil tends to behave as a viscous solid-fluid mixture of negligible shear strength, possibly unable to constrain pipeline movements. Therefore, pipelines may experience excessive displacement, for instance in the form of vertical flotation or sinking. To date, there are no well-established methods to predict pipe displacement in the event of liquefaction. To fill such a gap, this work proposes a computational fluid dynamics (CFD) framework enriched with soil mechanics principles. It is shown that the interaction between pipe and liquefied sand can be successfully analysed via one-phase Bingham fluid modelling of the soil. Post-liquefaction enhancement of rheological properties, viscosity and yield stress, can also be accounted for by linking soil-pipe CFD simulations to separate analysis of pore pressure dissipation. The proposed approach is thoroughly validated against the results of small-scale pipe flotation and pipe dragging tests from the literature.

INTRODUCTION

Pipeline infrastructure is widely employed in offshore energy developments to transport hydrocarbons from wells to plants for processing and distribution. When directly laid on the seabed, pipelines are often exposed to harsh hydrodynamic loads that may negatively impact their structural performance. Although pipelines can usually withstand large displacements, the set-up of suitable stabilization measures drives major costs in real projects (Cheuk et al., 2008; White and Cathie, 2010). A typical stabilization option is to lay pipelines in trenches back-filled with rocks or sand. Pipe trenching can be very expensive, but allows to increase lateral resistance and drastically reduce hydrodynamic forces (Teh et al., 2006; Bai and Bai, 2014).

Pipelines buried in sandy backfill may suffer from the consequences of soil liquefaction, since backfills are inevitably loose (uncompacted) and shallow (i.e., at low effective stresses). Liquefaction can be triggered by a number of factors, including structural vibrations, ocean waves, tidal fluctuations, and earthquakes (Sumer et al., 1999; De Groot et al., 2006; Luan et al., 2008). Due to the low strength and stiffness of fluidized soils, segments of buried pipelines may experience excessive displacements, for instance in the form of vertical flotation or sinking. In presence of light pipelines, the large unit weight of liquefied sand is often the main flotation trigger. Reportedly, pipes may also float during/after trench backfilling, due to soil liquefaction phenomena taking place behind the backfill plough (Cathie et al., 1996).

Following the first pioneering studies in the United States (Pipeline Flotation Research Council, 1966), North Sea offshore developments fostered in-depth research on how soil liquefaction can impact pipeline stability (Sumer et al., 1999; Damgaard and Palmer, 2001). Relevant outcomes of these research efforts are nowadays reflected by existing industry design guidelines (DNV, 2007a,b). As pipeline routes can hardly avoid all liquefiable areas, geotechnical input to pipeline design must include (i) assessment of liquefaction susceptibility (De Groot et al., 2006), and (ii) prediction of pipe displacement possibly induced by soil liquefaction (Bonjean et al., 2008; Erbrich and Zhou, 2017; Bizzotto et al., 2017).

This paper concerns the analysis of buried pipelines interacting with liquefied sand. A novel CFD-based approach is proposed to predict post-liquefaction pipe displacement, accounting for large deformations and re-consolidation effects in the soil. To prioritize applicability, large-deformation modelling of liquefied sand as a two-phase mixture was not pursued. Such endeavour was discouraged by the many questions still open about applying traditional soil mechanics to fluidized geomaterials. Instead, a one-phase approach was preferred, combining Bingham CFD modelling and separate analysis of pore pressure dissipation. As detailed in the following, the latter aspect enables to incorporate phenomenological enhancement of rheological soil properties in the 'early' post-liquefaction phase. While emphasis is on formulation and validation of the proposed framework, its applicability to both submarine and onshore infrastructures is noted – a relevant example of the latter case concerns, e.g., the seismic analysis of buried lifelines (Akiyoshi and Fuchida, 1984; Ling et al., 2003; Yasuda and Kiku, 2006; Chian and Madabhushi, 2012; Kruse et al., 2013).

CFD MODELLING OF LIQUEFIED SAND INTERACTING WITH BURIED PIPES

This section presents conceptual background and formulation of the proposed modelling approach, including critical discussion of relevant assumptions.

Conceptual background

Soil-structure interaction problems are usually tackled in the framework of continuum solid mechanics. Despite the particulate nature of soils, continuum theories have successfully supported general understanding of soil mechanics and its implications in geotechnical/structural design. Even the presence of pore fluid has been well accommodated in the same framework, owing to the notion of effective stress and the associated 'effective stress principle' (Terzaghi, 1943). When regarded as (continuum) solids, water-saturated soils exhibit frictional non-linear behaviour, and respond to external loads through deformations (both deviatoric and volumetric) that are strongly coupled with pore water flow. Typical design requirements in civil engineering have determined the wide success of small-deformation approaches along with soil plasticity modelling (Muir Wood, 2014).

The applicability of solid mechanics, however, should be questioned when external loading and hindered water drainage induce pore pressures that are large enough for the mean effective stress (p') to vanish. The occurrence of the latter event, most easily in shallow soil layers, has drastic implications: typical attributes of solid behaviour (grain contacts, shear strength and stiffness) disappear, while the soil begins to flow as a fluidized grain-water mixture. Such flow is nearly incompressible, rate-dependent, and inevitably associated with large deformations (Guoxing et al., 2016). It should be noted that the transition from solid-like to fluid-like state is not irreversible, as water drainage and pore pressure dissipation (so-called re-consolidation) can eventually re-establish grain contacts and frictional solid-like behaviour.

Recent research efforts have been spent to unify the constitutive modelling of granular materials in their solid, 'transitional' and fluid states (Andrade et al., 2012; Prime et al., 2014; Vescovi et al., 2019). However, application of such approaches to boundary value problems is still far from trivial, also due to dearth of numerical methods and software able to cope with two-phase media and deformations of any magnitude.

A practice-oriented approach is here proposed to analyse the interaction between buried pipes and liquefied sand. The following simplifying assumptions were formulated in light of relevant experimental evidence:

1. for practical purposes, it is possible to idealize liquefied sand as a one-phase, non-Newtonian viscous fluid, and analyse its flow using CFD (see the "CFD formulation and numerical solution" section, and equations therein);

2. at the onset of post-liquefaction re-consolidation, even moderate dissipation of pore pressure can significantly affect the behaviour of liquefied sand. Although genuinely hydro-mechanical, such mechanism can be phenomenologically captured within the same one-phase fluid framework through suitable variations of rheological properties (see Equations (4)–(5));

3. Post-liquefaction pore pressures needed for the update of liquefied sand's Bingham rheological properties can be separately estimated through two-phase, small-deformation analysis of re-consolidation (see Equations (11)–(12)).

Rheology of liquefied sand

The study of fluidized soils, including liquefied sand, has attracted numerous researchers with an interest in earthquake engineering (Seed et al., 1976; Stark and Mesri, 1992; Tamate and Towhata, 1999; Olson and Stark, 2002) and/or propagation of flow-slides and debris-flows (Pierson and Costa, 1987; Uzuoka et al., 1998; Parsons et al., 2001). Although their nature is intrinsically multi-phase, one-phase CFD modelling has gained wide popularity, e.g., for simplified simulation of debris avalanches (Boukpeti et al., 2012; Pastor et al., 2014) or seismic lateral spreading (Uzuoka et al., 1998; Hadush et al., 2000; Montassar and de Buhan, 2013). In fact, adopting a one-phase approach brings about significant modelling advantages while preserving, if properly implemented, features of behaviour relevant to engineering applications. The advantages of this approach include (i) simpler formulation of (one-phase) field equations and constitutive relationships (without 'two-way' hydro-mechanical coupling), (ii) reduced computational costs, and (iii) no numerical difficulties related to vanishing effective stresses when soil liquefaction occurs.

Soil-water mixtures with high solid concentration (i.e., beyond 35 % in volume) are most often modelled as non-Newtonian Bingham fluids (O'Brien and Julien, 1988). Accordingly, the relationship between deviatoric stress and strain rate tensors is assumed to be linear above a so-called 'yield stress', below which no flow occurs. In the case of one-dimensional shear flow, the Bingham model reads as a simple uniaxial relationship between shear stress (τ) and shear strain rate ($\dot{\gamma}$):

$$\begin{cases} \tau = \tau_y + \eta\dot{\gamma} \quad \text{if} \quad \tau > \tau_y \\ \\ \dot{\gamma} = 0 \quad \text{otherwise} \end{cases} \tag{1}$$

where η and τ_y represent viscosity and yield stress of the fluidized soil, respectively. In case of 2D/3D flow problems, multi-axial representation of stresses and strain rates is necessary:

$$\begin{cases} \sigma_{ij} = s_{ij} + p\delta_{ij} \\ \\ \dot{\varepsilon}_{ij} = \dot{e}_{ij} + \dfrac{\dot{\varepsilon}_{vol}}{3}\delta_{ij} \end{cases} \tag{2}$$

with the stress (σ_{ij}) and strain rate ($\dot{\varepsilon}_{ij}$) tensors decomposed into their deviatoric (s_{ij} and e_{ij}) and isotropic (p and $\dot{\varepsilon}_{vol}$) components – δ_{ij} is the second-order identity tensor. Accordingly, Equation (1) can be generalized as follows (Cremonesi et al., 2011):

$$\begin{cases} s_{ij} = \tau_y \dfrac{\dot{e}_{ij}}{\left\|\dot{e}_{ij}\right\|} + 2\eta \dot{e}_{ij} \quad \text{if} \quad \left\|s_{ij}\right\| > \tau_y \\ \\ \dot{e}_{ij} = 0 \quad \text{otherwise} \end{cases} \tag{3}$$

where $\left\|s_{ij}\right\| = \sqrt{(1/2)\, s_{ij} s_{ij}}$ and $\left\|\dot{e}_{ij}\right\| = \sqrt{(1/2)\, \dot{e}_{ij} \dot{e}_{ij}}$ are the norms of deviatoric stress and strain rate tensors, respectively. Total ($\dot{\varepsilon}_{ij}$) and deviatoric ($\dot{e}_{ij}$) strain rate tensors coincide in case of incompressible flow, i.e., when $\varepsilon_{vol} = 0$ at all times.

Decades of research have revealed broad variability of rheological parameters (Tamate and Towhata, 1999; Parsons et al., 2001; Hwang et al., 2006), particularly of viscosity. According to Montassar and de Buhan (2013), "obtained data for the equivalent Newtonian viscosity coefficients range between 10^{-1} and 10^{7} Pa·s". Not only 'intrinsic' factors (e.g., soil mineralogy, porosity, and grain size distribution) contribute to such variability, but also the lack of standard procedures for the interpretation of laboratory tests (Della Vecchia et al., 2019).

Enhancement of rheological properties during re-consolidation

The large permeability of sandy soils often enables water drainage soon after liquefaction. As a consequence, pore pressure dissipation and concurrent increase in mean effective pressure (p') gradually bring the soil back to its solid-like state (re-consolidation). The earliest stage of such transition is characterized by liquefied sand that still flows as a fluid, though with rheological behaviour directly affected by ongoing re-consolidation. Capturing this rapid process is relevant to the analysis of soil-structure interaction, for instance, during pipe flotation. To preserve the applicability of Bingham CFD modelling, quantitative information about post-liquefaction rheology (i.e., values and time evolution of rheological parameters) should be included in numerical calculations.

Data from experimental studies can be used in support of the above idea, i.e., to describe the dependence of η and τ_y on p' when $r_u < 1$ (Nishimura et al., 2002; Gallage et al., 2005; Towhata et al., 2010; Guoxing et al., 2016; Chen et al., 2013, 2014; Lirer and Mele, 2019) – r_u is the ratio between current pore pressure and pre-liquefaction effective mean stress p'_0. Particularly meaningful is the work of Gallage et al. (2005), who inferred Bingham properties by subjecting sand specimens at low p' to steps of axial compression at constant pore pressure. Figure 1 displays values of η and τ_y measured for low mean effective stress, with p' lower than 20 kPa – note that such low values are fully representative of soil effective stresses near the onset of liquefaction. Small increments in p' produce remarkable increase in η and τ_y, especially when compared to values extrapolated for $p' = 0$ ($r_u = 1$). All the tests performed by Gallage et al. (2005) show pronounced viscous behaviour at very low p', which corroborates the assumption of fluid-like sand behaviour also in the early post-liquefaction phase.

As for CFD modelling, the data in Fig. 1 suggest that both τ_y and η may be split into two components:

$$\tau_y = \tau_y^0 \left(r_u = 1\right) + \tau_y^{rec} \left(r_u, p'_0\right) \tag{4}$$

$$\eta = \eta^0 \left(r_u = 1\right) + \eta^{rec} \left(r_u, p'_0\right) \tag{5}$$

with τ_y^0 and η^0 material parameters related to fully liquefied conditions ($r_u = 1$), and τ_y^{rec} and η^{rec} variable components evolving during re-consolidation, i.e., as p' gradually increases from zero. τ_y^{rec} may be physically associated with recovery of shear strength:

$$\tau_y^{rec} = A_{\tau_y} p' \approx \frac{M}{\sqrt{3}} p' \tag{6}$$

Figure 1a supports the idea of linking the material coefficient A_{τ_y} to the critical stress ratio M of the fully re-consolidated soil, which lies in the $0.9 - 1.4$ range for friction angles between 25° and 35°. The factor $1/\sqrt{3}$ in (6) is consistent with the multi-axial formulation in (3) of a circular yield criterion in the deviatoric π-plane. It should also be noted that, as r_u decreases, τ_y^{rec} quickly grows much larger than τ_y^0, the latter being reported to be usually lower than 100 Pa in fully liquefied sand (O'Brien and Julien, 1988; Uzuoka et al., 1998; Parsons et al., 2001; Pierson, 2005).

The (rare) data in Figure 1b hints to adopt, as a first approximation, linear p'-dependence for η^{rec} as well:

$$\eta^{rec} = A_\eta p' \tag{7}$$

in which the material parameter A_η is unfortunately difficult to identify on a micromechanical basis. Figure 1b indicate A_η values in the range of 5 – 15 Pa·s/Pa.

CFD formulation and numerical solution

The interaction between buried pipe and liquefied sand has been studied throughout this work as a fluid-structure interaction problem. CFD simulations were performed using the Particle Finite Element Method (PFEM), in the version developed by Cremonesi et al. (2010, 2011) after Idelsohn et al. (2004). The PFEM has been widely applied to engineering applications, such as fluid dynamics (Idelsohn et al., 2004; Oñate et al., 2014a), fluid-structure interaction (Idelsohn et al., 2006; Franci et al., 2016; Zhu and Scott, 2014), bed erosion (Oñate et al., 2008), manufacturing processes (Oñate et al., 2014b), landslides (Cremonesi et al., 2017) and granular flows (Zhang et al., 2014), and recently simulation of cone penetration in water-saturated soils (Monforte et al., 2017). The PFEM adopts a fully Lagrangian description of free-surface fluid flow, especially suitable for fluid-structure interaction problems.

In a fully Lagrangian framework, conservation of linear momentum and mass must be fulfilled over the moving fluid volume Ω_t during the time interval $(0, T)$:

$$\begin{aligned} \rho \frac{Dv_i}{Dt} &= \sigma_{ij,j} + \rho b_i \quad \text{in } \Omega_t \times (0,T) \\ v_{i,i} &= 0 \quad \text{in } \Omega_t \times (0,T) \end{aligned} \tag{8}$$

where Dv_i/Dt represents material time differentiation applied to components of local velocity v_i, while σ_{ij}, ρ, and b_i stand for total (Cauchy) stress tensor, mass density, and external body force vector, respectively.

Following the PFEM, governing equations were discretized in space with linear interpolation functions for velocity and stress variables; backward Euler time integration was performed along with Newton-type step iterations. The inevitable mesh distortion associated with large deformations was remedied through a re-meshing procedure based on Delaunay tessellation (Cremonesi et al., 2010). A plane-strain 2D version of the above method was adopted.

The pipe was modelled as a rigid body, whose translation in time is governed by the following equilibrium equation:

$$\rho_p A_p \ddot{w}_i = \underbrace{W_i^p}_{\rho_p g_i A_p} + \underbrace{F_i^{fluid}}_{\int_{\Gamma_p} \sigma_{ij} n_j \, \mathrm{d}\Gamma_p} + \underbrace{F_i^{struct}}_{-K_{struct} w_i} \tag{9}$$

where w_i is the displacement vector of the pipe centroid, ρ_p and A_p the mass density and cross-section area of the pipe, and $[g_i] = [0 \quad 0 \quad -9.81]$ m/s^2 the gravity acceleration vector. The force terms on the right-hand side relate to pipe weight (W_i^p), interaction with the fluidized soil (F_{fluid}), and other structural restoring forces (F_i^{struct}), respectively. F_i^{fluid} represents the integral of fluid stresses (σ_{ij}) along the lateral surface of the pipe (Γ_p, with n_j its normal unit vector), and includes both buoyancy and drag effects. Whenever applicable, F_i^{struct} reflects the considered structural system, and was assumed to linearly depend on w through a (case-specific) elastic stiffness K_{struct}. The rotational degree of freedom is not relevant to the applications addressed in the following, and therefore not considered in Equation (9).

The interaction between pipe and liquefied sand was captured via a staggered Dirichlet-Neumann scheme (Cremonesi et al., 2010). At each time step, the velocity of the rigid body was applied to the fluid interface as a Dirichlet boundary condition; after solving the CFD problem in the surrounding fluid (Equation (8)), stresses along the pipe boundary were integrated to obtain the F_i^{fluid} term in Equation (9), and then update location and velocity of the pipe in the PFEM model. This staggered procedure was performed iteratively for each time-step until convergence (Figure 2). Overall, the proposed approach relies on the time-domain solution of Navier-Stokes equations (8) for an incompressible Bingham fluid, whose yield stress and viscosity are updated in space/time through Equations (4)–(7). Such update is based on current p' values obtained by separately solving the re-consolidation model described in the following. A synopsis of the proposed approach is provided in Figure 2.

Pore pressure dissipation during re-consolidation

The numerical solution of system (8) requires a suitable constitutive relationship between stresses and strain rates in the liquefied sand. To this end, Bingham modelling with evolving rheological parameters was adopted to capture re-consolidation effects in the early post-liquefaction phase. According to Equations (6)–(7), the enhancement of τ_y and η, depends on the current effective mean stress p', which is in fact not a variable in the one-phase CFD model. The analyses of soil-pipe interaction and pore pressure dissipation were therefore decoupled, with the latter reduced in practice to a 1D problem. This choice corresponds to assuming that the presence of the pipe does not severely affect the pore pressure field (as well as p') in the re-consolidating soil.

Pore pressure dissipation (re-consolidation) in a horizontal soil layer was simulated using Terzaghi's effective stress 1D theory (Terzaghi, 1943). Accordingly, the recovery of p' occurs at expense of the excess pore pressure u_e:

$$p'(z,t) = [1 - r_u(z,t)]\, p'_0 = -\Delta u_e(z,t) \tag{10}$$

for any time (t) and depth below the soil surface (z), starting from the initial condition $p'(z,0) = 0$ (fully liquefied soil layer). While the bulk of Terzaghi's theory was held valid, some changes were motivated by the highly non-linear behaviour of sand at very low p'. Indeed, a number of experimental studies show that, during re-consolidation, both hydraulic conductivity k and 1D oedometer stiffness E_{oed} ($= 1/m_v$, oedometer compressibility) depend strongly on the current effective stress level and void ratio (Brennan and Madabhushi, 2011; Haigh et al., 2012; Adamidis and Madabhushi, 2016).

The evolution of the excess pore pressure field $u_e(z,t)$ was simulated by solving the following diffusion equation (Adamidis and Madabhushi, 2016):

$$\frac{\partial u_e}{\partial t} = \frac{E_{oed}}{\gamma_w} \frac{\partial}{\partial z} \left(k \frac{\partial u_e}{\partial z} \right) \tag{11}$$

where γ_w represents the unit weight of pore water. Along with u_e, the evolution of the void ratio e (ratio of the volume of the voids to the volume of solids, and related to porosity as $\phi = e/(1+e)$) was also obtained as:

$$\frac{\partial e}{\partial t} = \frac{1+e}{E_{oed}}\frac{\partial u_e}{\partial t}. \tag{12}$$

The empirical relationship proposed by Adamidis and Madabhushi (2016) was adopted for the hydraulic conductivity:

$$k = C_T \frac{e^3}{(1+e)}\left[1 + 0.2\exp(-100\sigma'_v)\right] \tag{13}$$

in which C_T is a constitutive parameter, σ'_v the vertical effective stress (in kPa), and k is expressed in m/s. In agreement with empirical evidence (Haigh et al., 2012), explicit dependence of k on σ'_v appears in Equation (13).

A number of 'compression models' are available in the literature for the 1D oedometer stiffness, typically implying a power-law dependence on the vertical effective stress σ'_v. Among all, the well-established relationship proposed by Janbu (1963) and reappraised by Muir Wood (2009) was adopted:

$$\frac{E_{oed}}{\sigma'_{ref}} = \chi\left(\frac{\sigma'_v}{\sigma'_{ref}}\right)^{\alpha} \tag{14}$$

where σ'_{ref} is a reference effective stress value, and α and χ two dimensionless material parameters – $0 \leq \alpha \leq 1.5$ and $10^0 \leq \chi \leq 10^6$ (Muir Wood, 2009).

Equation (11) was solved in combination with common initial/boundary conditions:

– fully liquefied soil layer: $u_e(z,0) = (\gamma_{sat} - \gamma_w)\,z \Rightarrow \sigma'_v(z,0) = 0$

– perfectly draining top boundary: $u_e(0,t) = 0$

– impervious bottom boundary: $\dfrac{\partial u_e}{\partial z}(H,t) = 0$

where γ_{sat} and H are the saturated unit weight of the soil and the depth of the lower boundary, respectively.

SIMULATION OF PIPE FLOTATION IN LIQUEFIED SAND

Especially relevant to model validation are the recent tests performed at Deltares (Delft, The Netherlands) to study post-liquefaction pipe flotation (Horsten, 2016). Pipe flotation experiments were executed in a large container (length: 4 m, width: 2.5 m, depth: 1.2 m), equipped with a fluidization system at the bottom to create sand samples of low relative density, in the range $D_r = 20 - 40\%$. Ittebeck sand was used for this purpose, a uniform fine sand characterized by $G_s = 2.64$ (specific grain gravity), $D_{50} = 0.165$ mm (median grain diameter), $e_{max} = 0.868$ (maximum void ratio), $e_{min} = 0.527$ (minimum void ratio). Three different high-density polyethylene (HDPE) flexible pipes were employed, with different outer diameter and thickness. The experimental set-up sketched in Figure 3 featured a fixed-end pipe buried in a saturated sand layer – the clamped edge was introduced to more realistically represent a pipeline connected to an existing structure. Geometrical and mechanical properties of the three pipes are listed in Table 1. More details about the experimental set-up can be found in Horsten (2016) – see https://repository.tudelft.nl.

Calibration of re-consolidation model

In the original experimental work (Horsten, 2016), sand re-consolidation tests were performed prior to flotation experiments. Such tests were performed in a 0.6 m diameter cylindrical container filled with a 1.2 m thick layer of saturated loose sand, and liquefaction was induced by means of single peak vibrations brought about by a falling weight. Pore pressures were measured by five bespoke transducers placed along depth with 0.2 m regular spacing. Specific reference is made here to Sample #2, reportedly characterized by zero initial relative density (initial void ratio $e_0 \sim e_{max}$). The considered re-consolidation tests provided data useful for calibrating the pore pressure dissipation model described above. Required soil properties and model parameters were directly inferred from Horsten (2016) whenever possible – see Table 2, set 1.

Setting the parameter C_T in Equation (13) is crucial in that it governs the reference hydraulic conductivity $k_0 = k(\sigma'_v = 0)$, not directly measurable. A value of $C_T = 4 \cdot 10^{-4}$ m/s was selected (yielding $k_0 = 1.68 \cdot 10^{-4}$ m/s) to reproduce the timescale of pore pressure diffusion in the experiment. This value of C_T is about 1/5 of that suggested by Adamidis and Madabhushi (2016) for Hostun sand, reflecting the fact that the latter soil is significantly coarser ($D_{50} = 0.47$ mm, see Haigh et al. (2012)) and more permeable than Ittebeck sand ($D_{50} = 0.17$ mm, see Horsten (2016)).

Regarding the choice of σ'_{ref}, χ and α in Equation (14), Muir Wood (2009) provides some broad guidance. Suggested ranges for sand are $10^2 \leq \chi \leq 10^3$, while α varies from 0.2-0.3 (over-consolidated) to 0.4-0.8 (normally consolidated).

Reference stress $\sigma'_{ref} = 100$ kPa (recommended by Muir Wood (2009)) and exponent $\alpha = 1.15$ were set for Ittebeck sand. A mid-range value of $\chi = 5.2 \cdot 10^2$ was selected to complete parameter calibration.

In Figure 4a numerical simulations of u_e isochrones are compared to experimental measurements, while Figure 4b shows simulated and measured time evolution of u_e at four different depths. Both plots exhibit good agreement between computed and measured values. Further insight can be gained from Figure 5, showing computed isochrones of permeability (Figure 5a) and 1D oedometer stiffness (Figure 5b), respectively. In line with Adamidis and Madabhushi (2016), the overall change in k during re-consolidation is rather small, whilst E_{oed} experiences large variations. Computed stiffness values appear reasonably close to expected small-stress values for clean sand (cf. Lauder and Brown (2014), Haigh et al. (2012)). The performance of the non-linear pore pressure dissipation model is further discussed in Appendix I with respect to test results provided by Adamidis and Madabhushi (2016).

Pipe flotation tests

The three pipes in Table 1 were subjected to separate flotation tests (Horsten, 2016). In all cases, liquefaction of loose Ittebeck sand was achieved through the impact of a weight falling on the sidewall of the rigid container. Resulting displacements of the pipes were measured in time at several locations along their length. As explained in Appendix II, raw flotation measurements had first to be post-processed to eliminate the effects of spurious rotations caused by imperfect clamping (Horsten, 2016).

Flotation tests were numerically simulated using the proposed CFD framework. 2D plane-strain PFEM models were set up, with the soil domain discretized using linear triangular elements – see mesh in Figure 6. Velocity no-slip boundary conditions were imposed along all rigid walls, along with zero pressure at the top surface. Measured/simulated displacements in Figures 7–9 relate to the mid-section of each pipe (section 1 in Figure 3). Following Equation (9), the 3D effect of the clamped edge (Figure 3) was incorporated in 2D simulations as an elastic restoring force. The structural stiffness $K_{struct} = (17/384) \cdot L_p^4/E_p I_p$ associated with the mid-section of a cantilever pipe was identified based on standard structural analysis.

Figure 7 shows how the upward displacement of the 200 mm pipe evolved in time during the test on pipe 3 (line with square markers). As expected, the general flotation trend features gradual decrease in pipe velocity until full arrest, after about 15 seconds. The dashed horizontal line in the same figure ('no-soil equilibrium') represents the equilibrium that the same elastic cantilever would theoretically attain under self-weight and fluid buoyancy only. Such equilibrium allows to appreciate the influence of shear drag.

While the total mass density ρ was directly obtained from available measured soil data (Table 2, set 1), enhanced Bingham parameters (τ_y^0, η^0, A_{τ_y}, A_η) were calibrated against the experimental flotation curve in Fig. 7:

– to reduce arbitrarity in calibration, default values $\tau_y^0 = 0$ and A_{τ_y} ($M = 1.2$) were set. The former reflects the dominance of re-consolidation over the low shear strength at $r_u = 1$, the latter relates to an average (critical state) friction angle of 30°;

– initial viscosity $\eta^0 = \eta\,(r_u \approx 1) = 2200$ Pa·s was selected to capture pipe velocity at the onset of flotation;

– the last parameter A_η was identified to match general trend and final equilibrium of flotation during re-consolidation.

A very satisfactory agreement between experimental and numerical results was achieved for $\eta^0 = 2200$ Pa·s and A_η =20 Pa·s/Pa. The influence of A_η was also parametrically studied to highlight the influence of viscosity enhancement on the timing of pipe flotation (Figure 7). It is worth noting the good consistency between the set of identified parameters (Table 3) and previous inferences from Gallage et al. (2005)'s test results (Figure 1).

Comparing the timing of pipe flotation (Figure 7) and pore pressure dissipation (Figure 4) leads to recognize the substantial influence of early re-consolidation on the final displacement of pipe 3. Even though pore pressures dissipate only slightly in the first 30 seconds of the experiment (by about 100 Pa), non-negligible regains in yield stress and viscosity emerge from Equations (6)–(7).

With the same set of calibrated parameters, similar PFEM simulations were performed to predict the uplift experienced by the mid-sections of pipes 1 and 2. The corresponding plots in Figures 8–9 confirm very satisfactory agreement between experimental and numerical results. The proposed CFD model appears capable to accommodate different degrees of re-consolidation effects for pipes of different size, weight and stiffness.

SIMULATION OF LATERAL PIPE DRAGGING IN LIQUEFIED SAND

The proposed CFD framework was further validated against the lateral pipe dragging experiments presented by Towhata et al. (1999). Reference is made to a 1g physical model test in which a pipe embedded in extremely loose saturated sand was laterally dragged at constant elevation after full liquefaction induced by strong shaking of the container (see Section 2 of Towhata et al. (1999) for details). Towhata et al. (1999)'s experiment was carried out on Toyoura sand, reportedly characterized by $G_s = 2.65$, $D_{50} = 0.17$ mm, and initial void ratio $e_0 = 1.04$. A 30 mm diameter, 300 mm long model pipe was embedded at 300 mm depth (constant during pipe dragging) in a sand stack of 400 mm thickness. Pipe dragging was enforced during post-liquefaction pore pressure dissipation, while pure re-consolidation experiments on Toyoura sand (such as those in Fig. 4) were not performed.

Despite high experimental uncertainties and limitations in reported data (Towhata et al., 1999), the 1D re-consolidation model was rather easily calibrated, by deducing the initial soil's unit weight from e_0 and G_s, and selecting for Toyoura sand a value of $C_T = 4 \cdot 10^{-4}$. This is consistent with the value chosen for Ittebeck sand, which has the same particle mean diameter, and likely similar permeability. Soil parameters in Equation (14) were set within typical ranges after Muir Wood (2009) – see Table 2, set 3. Figure 10 shows the time evolution of simulated and measured excess pore pressure (at the top of the pipe), starting from initial full liquefaction. The beginning and end of pipe dragging are marked on the experimental curve. Pore pressure dissipation is globally well reproduced, although a slight offset between simulated and experimental curves is noticeable near when pipe dragging is arrested.

After calibrating the pressure dissipation model, enhanced Bingham parameters were identified for liquefied Toyoura sand. For this purpose, the experimental force-time curve obtained by Towhata et al. (1999) for a lateral dragging velocity of 8 mm/s and the same (pre-liquefaction) void ratio $e_0 = 1.04$ was used. The same values as above of τ_y^0 and A_{τ_y} were re-used to limit freedom in calibration, while η^0 and A_η were identified as follows:

- the initial viscosity $\eta^0 = \eta\,(r_u \approx 1) = 300$ Pa·s was selected to capture drag force values at the beginning of lateral dragging;
- the last parameter A_η was identified to reproduce the increase in drag force during re-consolidation.

PFEM simulations were set up with a pipe initially still for the first 4 s, allowing for some re-consolidation to occur before lateral dragging (Figure 10). In the absence of any structural connections, $F_i^{struct} = 0$ was set in Equation (9) for the laterally dragged pipe. Figure 11a shows satisfactory agreement between experimental and numerical curves in terms of drag force per unit length. The relevance of re-consolidation stands out when considering the result of a purely Newtonian simulation ($\tau_y^0 = A_{\tau_y} = A_\eta = 0$ and $\eta^0 = 300$ Pa·s): without regain in shear resistance, the drag force during pipe dragging at constant velocity would barely vary.

Identified Bingham parameters proved again consistent with existing knowledge on liquefied sand rheology. Particularly, the viscosity enhancement coefficient (A_η = 13 Pa·s/Pa) falls exactly within the range indicated by Gallage et al. (2005)'s data in Figure 1b, also very close to the value calibrated to reproduce Horsten (2016)'s flotation tests. The influence of A_η on the increase in drag force is parametrically demonstrated in Figure 11b. The same figure also shows that the effect of increasing viscosity (η^{rec}, Equation (5)) prevails over the regain of shear strength, as shown by the relatively low force associated with $A_\eta = 0$ (i.e., with increase in τ_y only). Although no specific calibration of A_{τ_y} was attempted, the tentative value in Table 3 is of the same order of magnitude as suggested by Gallage et al. (2005)'s data (Figure 1a).

The data in Towhata et al. (1999) provided for further model validation, regarding the relationship between drag force and dragging velocity. Experimental tests were performed for sand samples with $e_0 = 1.03 - 1.05$, and three different velocities – namely, 4, 8, 12 mm/s. Figure 12 illustrates the comparison between experimental and numerical results, showing satisfactory simulation of rate effects.

CONCLUDING REMARKS

This work presented a CFD-based approach to analyse the interaction between buried pipelines and liquefied sand, accounting for transient re-consolidation effects. Advanced PFEM simulations were performed in combination with enhanced Bingham modelling of the fluidized soil. The rheological enhancement consisted of an update in space and time of both viscosity and yield strength, based on separate non-linear analysis of pore pressure dissipation. The result was a Lagrangian CFD framework capable of dealing with large deformations and re-consolidation without explicit modelling of the transition from fluid-like to solid-like behaviour.

The soundness of the proposed approach and related calibration procedures were investigated with reference to the experimental literature regarding the interaction of buried pipes with liquefied sand. It was shown that capturing the regain in yield stress and viscosity induced by re-consolidation impacts positively the evaluation of interaction forces and/or displacements experienced by pipes moving through liquefied sand.

The main novelty of this work is the development of a practice-oriented, simplified numerical framework for the analysis of pipeline-soil interaction in the event of soil liquefaction, without the need to model phase transitions in multi-phase geomaterials. The main model limitations can be considered to be (i) the fact that the pore pressure diffusion model is one-dimensional, and (ii) the phenomenological nature of the proposed law expressing the variation of rheological parameters with pore pressure. Hence, further improvements may be achieved by (i) using 2D/3D pore pressure diffusion models to deal with more complex geometries and boundary conditions, and (ii) reinforcing the micromechanical link between viscosity enhancement and pore pressure dissipation.

The underlying large deformation approach is also expected to suit other flotation triggering mechanisms, e.g., those associated with underwater backfilling of pipeline trenches.

DATA AVAILABILITY

All data, models, or code that support the findings of this study are available from the corresponding author upon reasonable request. These include:

– numerical simulation results plotted in the manuscript;

– numerical code for soil-pipe CFD simulations;

– numerical code for pore pressure dissipation analysis.

ACKNOWLEDGEMENTS

Input from Omar Zanoli (*Rina Consulting*) is gratefully acknowledged, as well as the support to numerical simulations provided by former MSc students Francesco Bortolotto (*Studio Geotecnico Italiano*) and Kelys Betancur Iglesias (*Cathie Associates*).

References

Adamidis, O. and Madabhushi, G. (2016). "Post-liquefaction reconsolidation of sand." *Proc. R. Soc. A*, 472(2186), 20150745.

Akiyoshi, T. and Fuchida, K. (1984). "Soil-pipeline interaction through a frictional interface during earthquakes." *International Journal of Soil Dynamics and Earthquake Engineering*, 3(1), 27–34.

Andrade, J. E., Chen, Q., Le, P. H., Avila, C. F., and Evans, T. M. (2012). "On the rheology of dilative granular media: bridging solid- and fluid-like behavior." *Journal of the Mechanics and Physics of Solids*, 60(6), 1122–1136.

Bai, Q. and Bai, Y. (2014). *Subsea pipeline design, analysis, and installation*. Gulf Professional Publishing.

Bizzotto, T., Brown, M., Brennan, A., Powell, T., and Chandler, H. (2017). "Modelling of pipeline and cable flotation conditions." *Offshore Site Investigation Geotechnics 8th International Conference Proceeding*, Vol. 865, Society for Underwater Technology, 865–871.

Bonjean, D., Erbrich, C., and Zhang, J. (2008). "Pipeline flotation in liquefiable soil." *Proc. Annual Offshore Tech. Conf., Houston, Paper OTC*, Vol. 19668.

Boukpeti, N., White, D., and Randolph, M. (2012). "Analytical modelling of the steady flow of a submarine slide and consequent loading on a pipeline." *Géotechnique*, 62(2), 137.

Brennan, A. J. and Madabhushi, S. P. (2011). "Measurement of coefficient of consolidation during reconsolidation of liquefied sand." *Geotechnical Testing Journal*, 34(2), 139–146.

Cathie, D., Machin, J., and Overy, R. (1996). "Engineering appraisal of pipeline flotation during backfilling." *Offshore Technology Conference*, Offshore Technology Conference.

Chen, Y., Liu, H., and Wu, H. (2013). "Laboratory study on flow characteristics of liquefied and post-liquefied sand." *European Journal of Environmental and Civil Engineering*, 17(sup1), s23–s32.

Chen, Y., Wu, H., Sha, X., and Liu, H. (2014). "Laboratory tests on flow characteristics of pre-liquefied sand." *International Efforts in Lifeline Earthquake Engineering*, 600–607.

Cheuk, C., White, D., and Bolton, M. D. (2008). "Uplift mechanisms of pipes buried in sand." *Journal of geotechnical and geoenvironmental engineering*, 134(2), 154–163.

Chian, S. and Madabhushi, S. (2012). "Effect of buried depth and diameter on uplift of underground structures in liquefied soils." *Soil Dynamics and Earthquake Engineering*, 41, 181–190.

Cremonesi, M., Ferri, F., and Perego, U. (2017). "A basal slip model for lagrangian finite element simulations of 3d landslides." *International Journal for Numerical and Analytical Methods in Geomechanics*, 41, 30–53.

Cremonesi, M., Frangi, A., and Perego, U. (2010). "A lagrangian finite element approach for the analysis of fluid–structure interaction problems." *International Journal for Numerical Methods in Engineering*, 84(5), 610–630.

Cremonesi, M., Frangi, A., and Perego, U. (2011). "A lagrangian finite element approach for the simulation of water-waves induced by landslides." *Computers & Structures*, 89(11-12), 1086–1093.

Damgaard, J. and Palmer, A. (2001). "Pipeline stability on a mobile and liquefied seabed: A discussion of magnitudes and engineering implications." *OMAE 2001: Proceedings of the 20th International Conference on Offshore Mechanics and Arctic Engineering, Rio de Janeiro, Brazil*, Vol. 4, American Society of Mechanical Engineers, 195–204.

De Groot, M., Bolton, M., Foray, P., Meijers, P., Palmer, A., Sandven, R., Sawicki, A., and Teh, T. (2006). "Physics of liquefaction phenomena around marine structures." *Journal of waterway, port, coastal, and ocean engineering*, 132(4), 227–243.

Della Vecchia, G., Cremonesi, M., and Pisanò, F. (2019). "On the rheological characterisation of liquefied sands through the dam-breaking test." *International Journal for Numerical and Analytical Methods in Geomechanics*, 43(7), 1410–1425.

DNV (2007a). "Global buckling of submarine pipelines–structural design due to high temperature/high pressure." *RP-F110, Oslo, Norway*.

DNV (2007b). "On-bottom stability design of submarine pipelines." *Det Norske Veritas (DNV), Oslo, Norway. DNV-RPF109*.

Erbrich, C. and Zhou, H. (2017). "Optimised backfill design for preventing pipeline flotation." *Offshore Site Investigation Geotechnics 8th International Conference Proceeding*, Vol. 872, Society for Underwater Technology, 872–880.

Franci, A., Oñate, E., and Carbonell, J. (2016). "Unified lagrangian formulation for solid and fluid mechanics and fsi problems." *Computer Methods in Applied Mechanics and Engineering*, 298, 520–547.

Gallage, C. P. K., Towhata, I., and Nishimura, S. (2005). "Laboratory investigation on rate-dependent properties of sand undergoing low confining effective stress." *Soils and foundations*, 45(4), 43–60.

Guoxing, C., Enquan, Z., Zhihua, W., Binghui, W., and Xiaojun, L. (2016). "Experimental investigation on fluid characteristics of medium dense saturated fine sand in pre-and post-liquefaction." *Bulletin of Earthquake Engineering*, 14(8), 2185–2212.

Hadush, S., Yashima, A., and Uzuoka, R. (2000). "Importance of viscous fluid characteristics in liquefaction induced lateral spreading analysis." *Computers and Geotechnics*, 27(3), 199–224.

Haigh, S. K., Eadington, J., and Madabhushi, S. P. G. (2012). "Permeability and stiffness of sands at very low effective stresses." *Geotechnique*, 62(1), 69–75.

Horsten, T. (2016). "Pipe uplift in liquefied sands." M.S. thesis, Delft University of Technology, Netherlands.

Hwang, J.-I., Kim, C.-Y., Chung, C.-K., and Kim, M.-M. (2006). "Viscous fluid characteristics of liquefied soils and behavior of piles subjected to flow of liquefied soils." *Soil Dynamics and Earthquake Engineering*, 26(2), 313–323.

Idelsohn, S., Oñate, E., and Pin, F. D. (2004). "The particle finite element method: a powerful tool to solve incompressible flows with free-surfaces and breaking waves." *International Journal for Numerical Methods in Engineering*, 61, 964–989.

Idelsohn, S., Oñate, E., Pin, F. D., and Calvo, N. (2006). "Fluid-structure interaction using the particle finite element method." *Computer methods in applied mechanics and engineering*, 195, 2100–2113.

Janbu, N. (1963). "Soil compressibility as determined by oedometer and triaxial tests." *Proceedings of the 3rd European conference on Soil Mechanics and Foundation Engineering*, Vol. 1, 19–25.

Kruse, H., Meijers, P., Costa Ferrer, C., de Lange, G., Vermaas, T., Havinga, H., Landwehr, J., and Heinsbroek, A. (2013). "Effects of induced earthquakes on the Gasunie network in groningen (in Dutch)." *Report no.*, Deltares.

Lauder, K. L. and Brown, M. J. (2014). "Scaling effects in the 1 g modelling of offshore pipeline ploughs." 377–383.

Ling, H. I., Mohri, Y., Kawabata, T., Liu, H., Burke, C., and Sun, L. (2003). "Centrifugal modeling of seismic behavior of large-diameter pipe in liquefiable soil." *Journal of geotechnical and geoenvironmental engineering*, 129(12), 1092–1101.

Lirer, S. and Mele, L. (2019). "On the apparent viscosity of granular soils during liquefaction tests." *Bulletin of Earthquake Engineering*, 1–16.

Luan, M., Qu, P., Jeng, D.-S., Guo, Y., and Yang, Q. (2008). "Dynamic response of a porous seabed–pipeline interaction under wave loading: soil–pipeline contact effects and inertial effects." *Computers and Geotechnics*, 35(2), 173–186.

Monforte, L., Arroyo, M., Carbonell, J. M., and Gens, A. (2017). "Numerical simulation of undrained insertion problems in geotechnical engineering with the particle finite element method (pfem)." *Computers and Geotechnics*, 82, 144–156.

Montassar, S. and de Buhan, P. (2013). “Numerical prediction of liquefied ground characteristics from back-analysis of lateral spreading centrifuge experiments.” *Computers and Geotechnics*, 52, 7 – 15.

Muir Wood, D. (2009). *Soil mechanics: a one-dimensional introduction*. Cambridge University Press.

Muir Wood, D. (2014). *Geotechnical modelling*. CRC press.

Nishimura, S., Towhata, I., and Honda, T. (2002). “Laboratory shear tests on viscous nature of liquefied sand.” *Soils and Foundations*, 42(4), 89–98.

O’Brien, J. S. and Julien, P. Y. (1988). “Laboratory analysis of mudflow properties.” *Journal of hydraulic engineering*, 114(8), 877–887.

Olson, S. M. and Stark, T. D. (2002). “Liquefied strength ratio from liquefaction flow failure case histories.” *Canadian Geotechnical Journal*, 39(3), 629–647.

Oñate, E., Franci, A., and Carbonell, J. (2014a). “Lagrangian formulation for finite element analysis of quasi-incompressible fluids with reduced mass losses.” *International Journal for Numerical Methods in Fluids*, 74 (10), 699–731.

Oñate, E., Franci, A., and Carbonell, J. (2014b). “A particle finite element method for analysis of industrial forming processes.” *Computational Mechanics*, 54, 85–107.

Oñate, E., Idelsohn, S., Celigueta, M., and Rossi, R. (2008). “Advances in the particle finite element method for the analysis of fluidmultibody interaction and bed erosion in free surface flows." *Computer methods in applied mechanics and engineering*, 197 (19-20), 1777–1800.

Parsons, J. D., Whipple, K. X., and Simoni, A. (2001). "Experimental study of the grain-flow, fluid-mud transition in debris flows." *The Journal of Geology*, 109(4), 427–447.

Pastor, M., Blanc, T., Haddad, B., Petrone, S., Morles, M. S., Drempetic, V., Issler, D., Crosta, G., Cascini, L., Sorbino, G., et al. (2014). "Application of a sph depth-integrated model to landslide run-out analysis." *Landslides*, 11(5), 793–812.

Pierson, T. C. (2005). "Hyperconcentrated flow—transitional process between water flow and debris flow." *Debris-flow hazards and related phenomena*, Springer, 159–202.

Pierson, T. C. and Costa, J. E. (1987). "A rheologic classification of subaerial sediment-water flows." *Reviews in Engineering Geology*, 7, 1–12.

Pipeline Flotation Research Council (1966). "ASCE preliminary research on pipeline flotation: Report of the pipeline flotation research council." *Journal of the Pipeline Division*, 92(1), 27–74.

Prime, N., Dufour, F., and Darve, F. (2014). "Solid–fluid transition modelling in geomaterials and application to a mudflow interacting with an obstacle." *International Journal for Numerical and Analytical Methods in Geomechanics*, 38(13), 1341–1361.

Seed, H. B., Martin, P. P., and Lysmer, J. (1976). "Pore-water pressure changes during soil liquefaction." *Journal of Geotechnical and Geoenvironmental Engineering*, 102(Proc. Paper# 12074).

Stark, T. D. and Mesri, G. (1992). "Undrained shear strength of liquefied sands for stability analysis." *Journal of Geotechnical Engineering*, 118(11), 1727–1747.

Sumer, B. M., Fredsøe, J., Christensen, S., and Lind, M. (1999). "Sinking/floatation of pipelines and other objects in liquefied soil under waves." *Coastal Engineering*, 38(2), 53–90.

Tamate, S. and Towhata, I. (1999). "Numerical simulation of ground flow caused by seismic liquefaction." *Soil Dynamics and Earthquake Engineering*, 18(7), 473–485.

Teh, T., Palmer, A., Bolton, M., and Damgaard, J. (2006). "Stability of submarine pipelines on liquefied seabeds." *Journal of waterway, port, coastal, and ocean engineering*, 132(4), 244–251.

Terzaghi, K. (1943). "Theoretical soil mechanics. johnwiley & sons." *New York*, 11–15.

Towhata, I., Anh, T. T. L., Yamada, S., Motamed, R., and Kobayashi, Y. (2010). "Zero-gravity triaxial shear tests on mechanical properties of liquefied sand and performance assessment of mitigations against large ground deformation." *Proceedings of 5th International Conference on Recent Advances in Geotechnical Earthquake Engineering and Soil Dynamics, San Diego, USA*.

Towhata, I., Vargas-Monge, W., Orense, R., and Yao, M. (1999). "Shaking table tests on subgrade reaction of pipe embedded in sandy liquefied subsoil." *Soil Dynamics and Earthquake Engineering*, 18(5), 347 – 361.

Uzuoka, R., Yashima, A., Kawakami, T., and Konrad, J.-M. (1998). "Fluid dynamics based prediction of liquefaction induced lateral spreading." *Computers and Geotechnics*, 22(3-4), 243–282.

Vescovi, D., Marveggio, P., and di Prisco, C. G. (2019). "Saturated granular flows: constitutive modelling under steady simple shear conditions." *Géotechnique*, 1–39.

White, D. and Cathie, D. (2010). "Geotechnics for subsea pipelines." *Proceedings of the 2nd International Symposium on Frontiers in Offshore Geotechnics, Perth*, 87–123.

Yasuda, S. and Kiku, H. (2006). "Uplift of sewage manholes and pipes during the 2004 niigataken-chuetsu earthquake." *Soils and Foundations*, 46(6), 885–894.

Zhang, X., Krabbenhoft, K., and Sheng, D. (2014). "Particle finite element analysis of the granular column collapse problem." *Granular Matter*, 16, 609–619.

Zhu, M. and Scott, M. H. (2014). "Modeling fluid-structure interaction by the particle finite element method in opensees." *Computers and Structures*, 132, 12–21.

Appendix I. FURTHER VALIDATION OF THE PORE PRESSURE DISSIPATION MODEL

The above pore pressure dissipation model was further tested against the measurements recorded by Adamidis and Madabhushi (2016) during re-consolidation centrifuge tests on Hostun sand – experiment OA2-EQ2. Selected parameters for this case are given in Table 2 – set 2, most of which taken from published values. Mid-range values for sand were assigned to χ and α following Muir Wood (2009). Simulated pore pressure isochrones and time profiles are compared in Figure 13 to experimental data. Despite the simplicity of the 1D stiffness model (14), all key features of re-consolidation are adequately captured.

Although all lying within expected ranges, the two parameter sets in Table 2 exhibit differences due to the sand type and, likely, to the adopted physical modelling strategy (1g vs centrifuge modelling).

Appendix II. CORRECTION OF RAW FLOTATION DATA

The original work of Horsten (2016) reported imperfect clamping of the pipe cantilever (Figure 3). As a consequence of such imperfection, all pipes experienced a component of rigid rotation during flotation, on average of about 0.9° – i.e., approximately 20 mm of additional displacement at the mid-section. This effect is readily visible in the raw displacement data provided by Horsten (2016) and plotted in Figure 14. In order to simplify PFEM simulations, it was decided to post-process the raw measured data and eliminate the effect of undesired rigid rotation. In all cases, it was straightforward to identify and remove the affected branch in each flotation curve, indicated in Figure 14 as 'end of clamp rotation'. Relevant bending was assumed to begin for each pipe at the end of rigid rotation, and corresponds with the corrected experimental data plotted in Figures 7–9. To approximate actual experimental conditions, PFEM simulations were set up with initial conditions consistent with the after-rotation configuration – i.e., including higher initial elevation of the pipe, non-zero initial velocity and sand re-consolidation already developed to some extent.

LIST OF SYMBOLS

Latin symbols

A_p = pipe cross-section area

A_{τ_y} = constitutive parameter accounting for yield stress enhancement during re-consolidation

A_η = constitutive parameter accounting for viscosity enhancement during re-consolidation

b_i = body force vector

C_T = hydraulic conductivity parameter

D_p = pipe diameter

D_r = relative density

D_{50} = median soil particle diameter

e = void ratio

e_{min} = minimum void ratio

e_{max} = maximum void ratio

E_{oed} = 1D oedometer stiffness

E_p = pipe Young modulus

$\dot{e}_{ij}$ = deviatoric strain rate tensor

g_i = gravity acceleration vector

F_i^{fluid} = fluid force on the pipe (per unit length)

F_i^{struct} = structural restoring force on the pipe (per unit length)

G_s = relative unit weight of soil grains

h_p = pipe elevation

H = thickness of the consolidating layer

I_p = moment of inertia of pipe cross-section

k = hydraulic conductivity

L_p = pipe length

M = soil critical stress ratio

m_v = 1D oedometer compressibility

n_i = unit vector normal to lateral surface of the pipe

p = mean total stress

p' = mean effective stress

p'_0 = initial mean effective stress

r_u = ratio between current pore pressure and initial mean effective stress

s_{ij} = deviatoric stress tensor

t = time

t_p = pipe thickness

T = end time of soil-pipe simulations

u_e = excess pore water pressure

v_i = velocity vector in the soil domain

w_i = pipe displacement vector

W_p = pipe weight (per unit length)

z = depth below soil surface

Greek symbols

α = soil stiffness parameter

χ = soil stiffness parameter

δ_{ij} = Kronecker identity tensor

$\dot{\varepsilon}_{ij}$ = strain rate tensor

$\dot{\varepsilon}_{vol}$ = volumetric strain rate

$\dot{\gamma}$ = shear strain rate

γ_w = water unit weight

Γ_p = pipe perimeter

η = viscosity

η^0 = viscosity of fully liquefied soil

η^{rec} = viscosity enhancement during re-consolidation

ϕ = porosity

ρ = soil mass density

ρ_p = pipe mass density

σ_{ij} = Cauchy stress tensor

σ'_r = radial component of the effective stress

σ'_v = vertical component of the effective stress

σ'_{ref} = reference effective stress

τ = shear stress

τ_y = yield stress

τ_y^0 = yield stress of fully liquefied soil

τ_y^{rec} = yield stress enhancement during re-consolidation

Ω_t = moving fluid volume

List of Tables

	h_p [mm]	L_p [m]	t_p [mm]	D_p [mm]	A_p [m^2]	I_p [m^4]
pipe 1	790	3	17	110	0.005	$3.5 \cdot 10^{-6}$
pipe 2	640	3	33	160	0.013	$1.6 \cdot 10^{-5}$
pipe 3	500	3	33	200	0.017	$2.3 \cdot 10^{-5}$
ρ_p = 950 kg/m^3 E_p = 1100 MPa						

Table 1. Pipe geometrical/mechanical properties – h_p = pipe elevation, L_p = length, t_p = cross-section thickness, D_p = outer diameter, A_p = cross-section area, I_p = cross-section moment of inertia, ρ_p = HDPE mass density, E_p = HDPE Young's modulus.

	H	γ	C_T	e_0	χ	α	σ'_{ref}
	[m]	[kN/m^3]	[m/s]	[–]	[–]	[–]	[kPa]
set 1	1.2	18.4	$4 \cdot 10^{-4}$	0.88	$7.3 \cdot 10^2$	1.15	100
set 2	12	18.7	$1.94 \cdot 10^{-3}$	0.84	$2.8 \cdot 10^2$	0.45	100
set 3	0.4	17.7	$4 \cdot 10^{-4}$	1.04	$0.2 \cdot 10^2$	0.5	100

Table 2. Re-consolidation model parameters used to reproduce experimental measurements from Horsten (2016) (set 1), Adamidis and Madabhushi (2016) (set 2) and Towhata et al. (1999) (set 3).

	τ_y^0 [kPa]	η^0 [Pa·s]	A_{τ_y} [–]	A_η [Pa·s/Pa]
pipe flotation	0	2200	0.6928	20
pipe dragging	0	300	0.6928	13

Table 3. Enhanced Bingham parameters used to reproduce measurements from pipe flotation (Horsten, 2016) and pipe dragging (Towhata et al., 1999) tests.

List of Figures

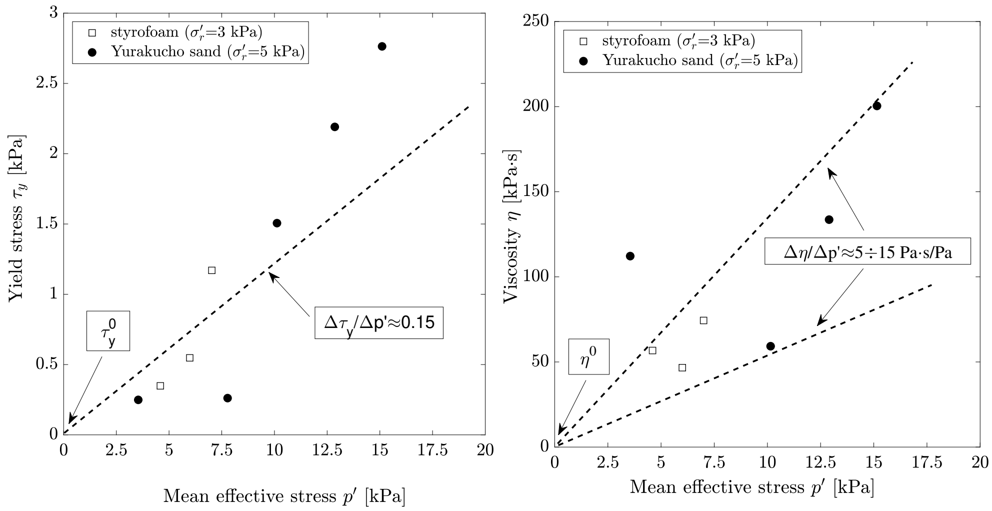

(a) p'–dependent yield stress

(b) p'–dependent viscosity

Figure 1. Dependence of Bingham parameters on mean effective stress, after Gallage et al. (2005) – pre-liquefaction relative density $D_r \approx 30\%$, σ'_r stands for radial effective stress.

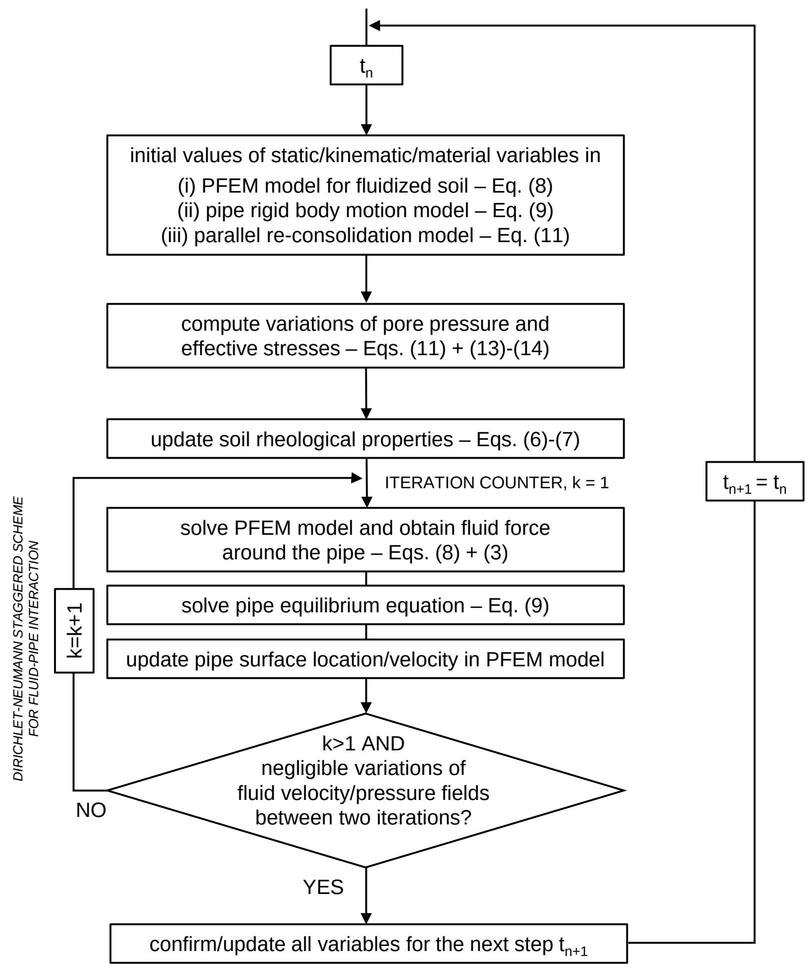

Figure 2. Solution of a single step in the proposed pipe-soil interaction algorithm.

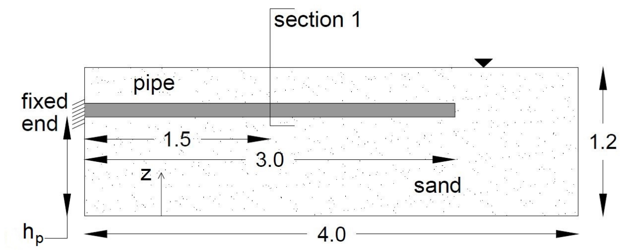

Figure 3. Skectch of Deltares' experimental set-up (Horsten, 2016) – dimensions in metres.

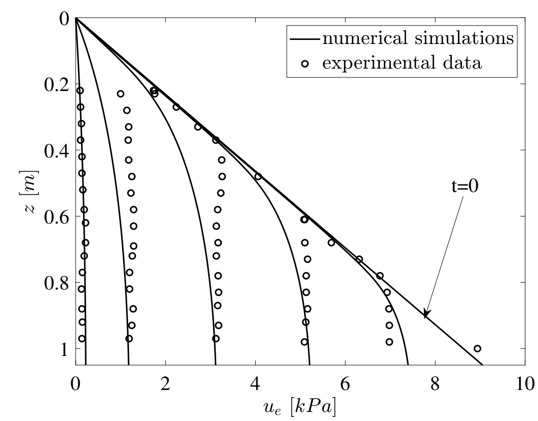

(a) u_e isochrones (plotted every 20 s)

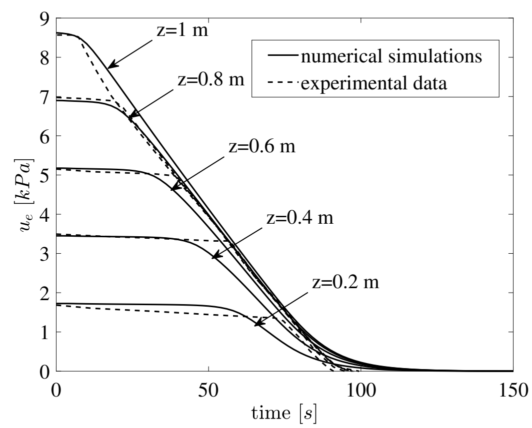

(b) u_e time profiles

Figure 4. Simulation of u_e dissipation – data from Horsten (2016), Sample #2.

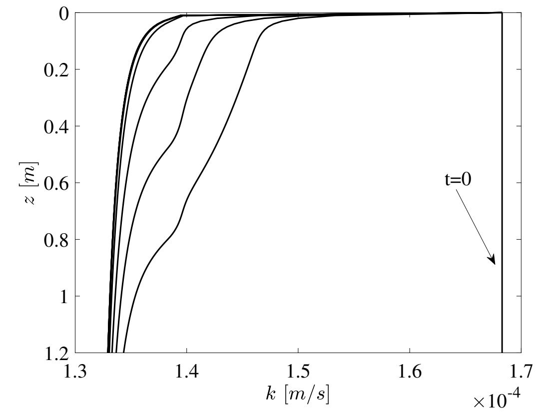

(a) permeability isochrones (plotted every 20 s)

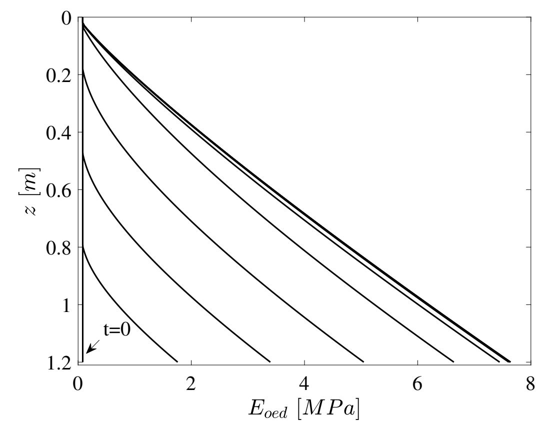

(b) oedometer stiffness isochrones (plotted every 20 s)

Figure 5. Isochrones of sand permeability and oedometer stiffness from the simulation of Horsten (2016)'s re-consolidation test on Sample #2.

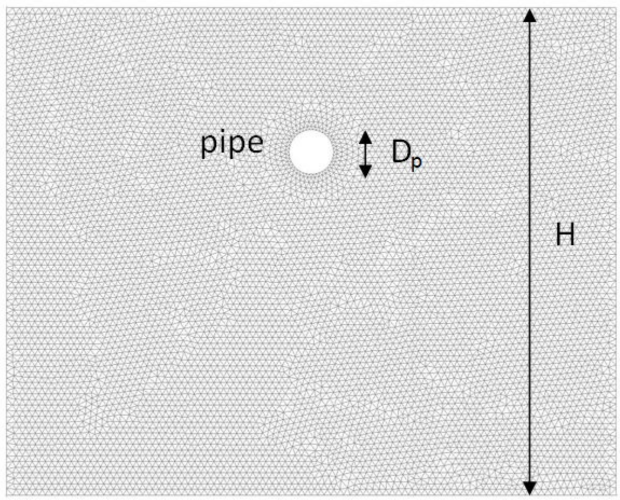

Figure 6. PFEM mesh for the simulation of pipe 1's flotation (Table 1).

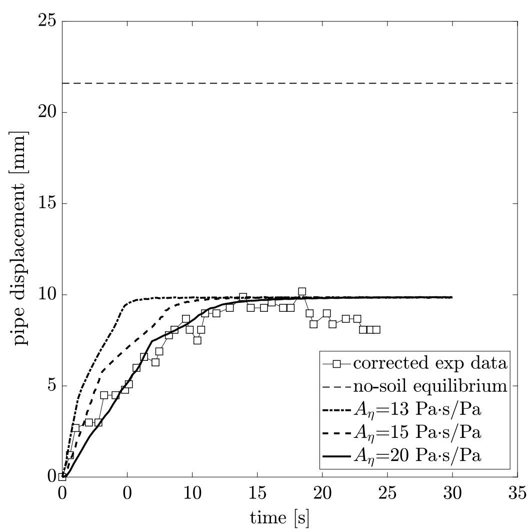

Figure 7. Pipe 3's flotation: comparison between CFD results and experimental data from Horsten (2016). Theoretical 'no-soil equilibrium' displacement: 21.7 mm.

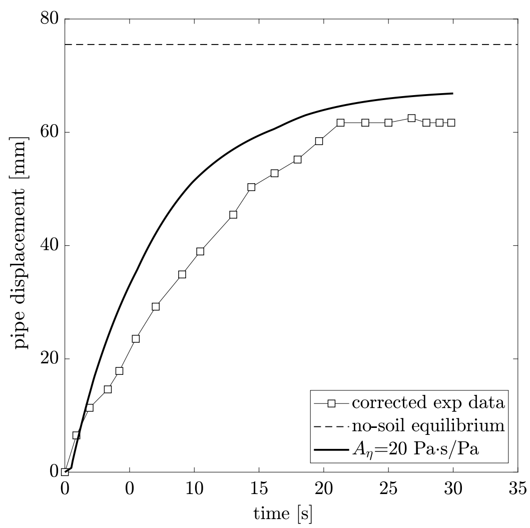

Figure 8. Pipe 1's flotation: comparison between CFD results and experimental data from Horsten (2016). Theoretical 'no-soil equilibrium' displacement: 75.5 mm.

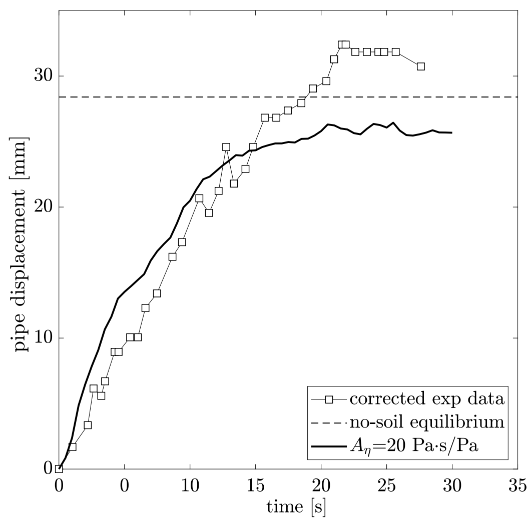

Figure 9. Pipe 2's flotation: comparison between CFD results and experimental data from Horsten (2016). Theoretical 'no-soil equilibrium' displacement: 28.4 mm.

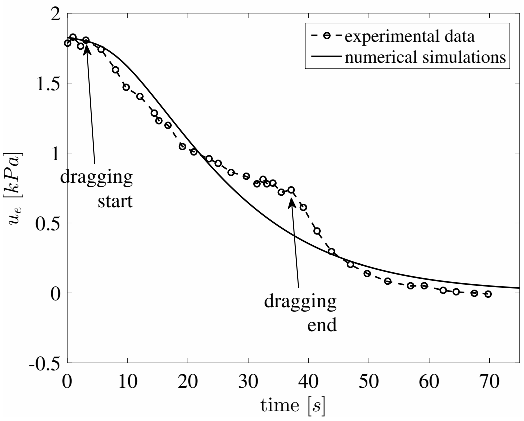

Figure 10. Simulation of u_e dissipation during pipe lateral dragging – data from Towhata et al. (1999).

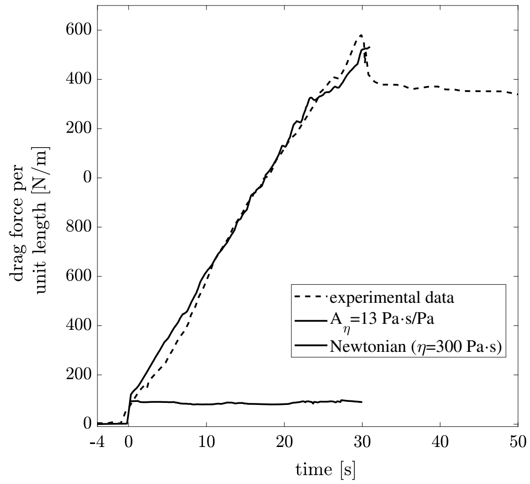

(a) calibration of the enhanced Bingham model

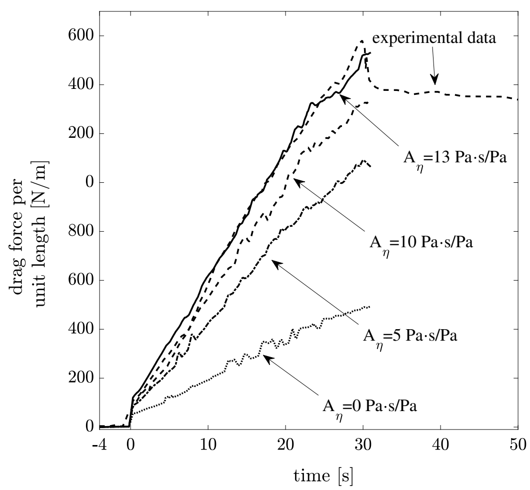

(b) influence of the A_η parameter

Figure 11. Lateral pipe dragging: comparison between results from experiments and enhanced Bingham simulations at constant dragging velocity (8 mm/s) and e_0 = 1.04 – data from Towhata et al. (1999).

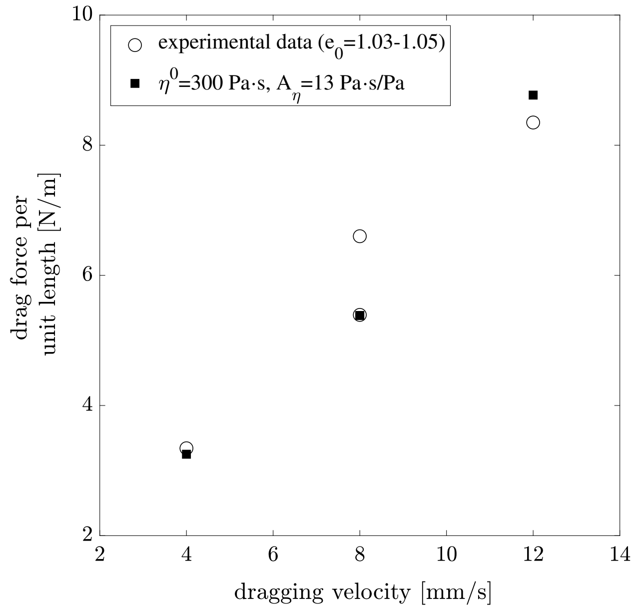

Figure 12. Lateral pipe dragging: influence of pipe velocity on drag force prior to reconsolidation ($r_u \approx 1$) – data from Towhata et al. (1999).

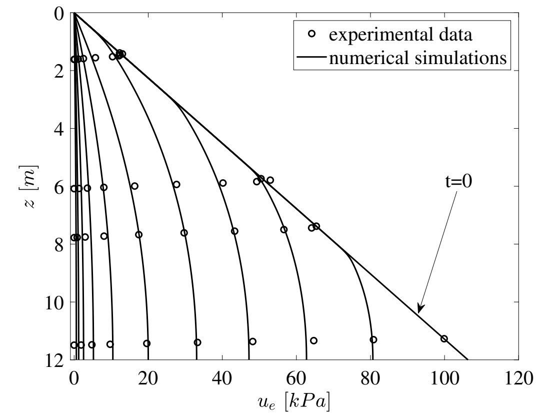

(a) u_e isochrones (plotted every 20 s)

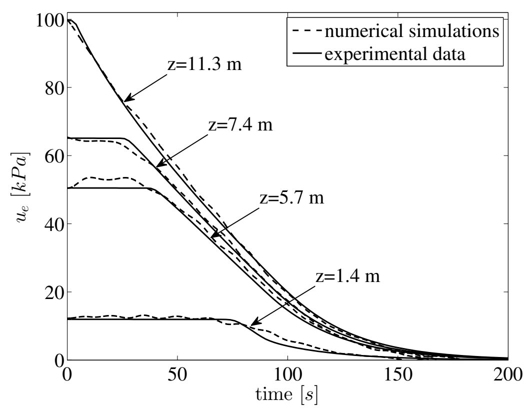

(b) u_e time profiles

Figure 13. Simulation of u_e dissipation – data from Adamidis and Madabhushi (2016), test OA2-EQ2.

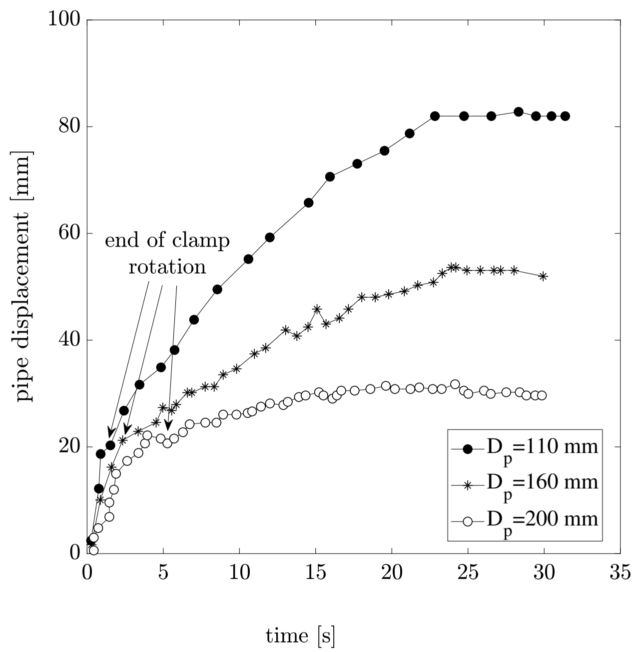

Figure 14. Raw flotation curves for pipes 1, 2, 3 – data from Horsten (2016).